Progress in Photovoltaics: Research and Applications

WILEY

PROGRESS IN PHOTOVOLTAICS

SPECIAL ISSUE ARTICLE OPEN ACCESS

Impact of Rapid Thermal Processing on Bulk Lifetime and Surface Recombination Velocity of Crystalline Silicon With Passivating Tunnel Oxide Contacts

F.-J. Haug | A. Morisset | M. Lehmann | S. Libraro | E. Genç | J. Hurni | C. Ballif

EPFL, PV-Lab, Neuchâtel, Switzerland

Correspondence: F.-J. Haug (franz-josef.haug@epfl.ch)

Received: 24 June 2024 | **Revised:** 20 November 2024 | **Accepted:** 13 January 2025

Funding: This work has received funding from the Swiss Federal Office for Energy (OFEN) within the project iPrecise (No. SI/502115-01) and the Swiss National Science Foundation (SNF) within the projects NACHOS (No. 200021L_172924/1) and IMPACT (no. 200021_185064). We acknowledge the support from the research and innovation program Horizon 2020 of the European Union within the Marie Skłodowska-Curie grant SLICE (No. 101028491), and we thank the Swiss State Secretariat for Research and Innovation (SERI) for funding the association to the EU-project APOLLO (No. 101122277).

Keywords: defect passivation | passivating contacts | rapid thermal processing | silicon solar cells | tunnel oxide

ABSTRACT

We investigate rapid thermal processing (RTP) as alternative to the prolonged thermal annealing process used to form tunnel-oxide passivating contacts for silicon solar cells. The thermal treatment is generally followed by hydrogenation to passivate defects at the Si/SiOx interface. Whereas industrial manufacturing generally uses Cz wafers, research is often carried out with FZ wafers. Both types of wafers are prone to the formation of thermal defects in the bulk. To disentangle effects of the interface and the bulk, we assess the lifetime at different steps of the process sequence for both wafer types. We find that the initial bulk lifetime of our *p*-type FZ material is maintained for RTP up to temperatures of about 450°C, followed by a severe decay and eventually a moderate extent of recovery at temperatures above 800°C. Compared to FZ material, the initial bulk lifetimes in our *p*-type Cz material are slightly lower, but they are maintained on that level up to about 600°C. Beyond that temperature, the lifetimes also decay, but to a lesser extent than in the FZ material, and there is no curing at higher temperatures. Hydrogenation can partially passivate the bulk defects in FZ material, but the initial state is not recovered. In Cz material, it appears that RTP creates two different types of defects; for those created up to 800°C, the initial state can be recovered by hydrogenation whereas those created at higher temperature cannot be passivated by hydrogenation. We also investigate the formation of *n*-type passivating contacts by RTP, and we fabricate solar cell precursors with a single RTP step and the same hydrogenation for both contact polarities. After sputtering a transparent conducting ITO layer on the full area and an Ag metallization, we achieve solar cells efficiencies up to 20.5%.

1 | Introduction

The use of passivating contacts has become key to high device efficiency in silicon solar cells. They can be made either with bilayers of intrinsic and doped amorphous silicon [1] or with a passivating tunnelling layer of SiOx in combination with doped poly-silicon [2]. Industrialization of these cell types demonstrated impressive progress reaching efficiencies of 26.8% and 25.6%, respectively [3]. Whereas industrial manufacturing generally uses Cz wafers, research is often carried out with FZ

[Correction added on 03 September 2025, after first online publication: The copyright line was changed.]

This article belongs to the WCPEC-8 Special issue published in issue 31:12 (WCPEC-8: Progress in Photovoltaics: Research and Applications: Vol 31, No 12).

wafers that might be prone to the formation of thermal defects [4, 5]. As the formation of passivating contacts involves a thermal treatment to crystallize the doped layer and to activate its dopants, it is of interest to characterize passivating contacts not only in terms of surface passivation, but also to monitor potential modifications in the bulk of the different wafer materials.

In this contribution, we build on earlier work on *p*-type FZ wafers [6], and we extend it to *p*-type Cz material; ongoing work on *n*-type material relevant for TOPCon cells will be covered elsewhere. We investigate how the thermal treatment during formation of passivating tunnel oxide contacts impacts properties of the bulk and of the interface, how both types of defects respond to hydrogenation.

2 | Experimental

We study passivating contacts on *p*-type FZ and Cz material. The wafers have resistivities of 2 Ωcm, they are 100 oriented, and their surfaces are either shiny etched (FZ) or saw-damage etched (Cz). Subsequent processing steps are shown in Figure 1; after standard cleaning, ~1.2-nm-thick interfacial oxides were formed by immersion in hot HNO_3. For some samples, the oxide layers were formed by exposure to N_2O plasma [7, 8] in a parallel plate reactor (Kai-M, Unaxis). Subsequently, 30-nm-thick layers of in situ doped amorphous silicon were grown symmetrically on both sides in the same reactor by plasma enhanced chemical vapour deposition (PECVD). We used a precursor gas mix of silane (SiH_4) and hydrogen (H_2). A small amount of methane (CH_4) was added to enhance adhesion, resulting in SiCx layers with carbon content between 1 and 3 at%. The in situ doping was achieved by adding either tri-methyl-boron ($B(CH_3)_3$, TMB) for *p*-type layers or phosphine (PH_3) for *n*-type layers. To crystallize the layers and to activate their dopants, we used rapid thermal processing (RTP) in Ar ambient at temperatures up to 930°C (Jetfirst 200, Jipelec). We use a pyrometer to control heating and cooling ramps of 50°C/s and a dwell time of 3 s; occasionally longer dwell times of 8 or 30 s were used. Following the thermal treatment, the samples were hydrogenated by depositing a 100-nm-thick layer of SiNx:H on both sides by MW-PECVD (MAiA, Meyer Burger), firing at a set temperature of 820°C to release hydrogen from the nitride (Camini, Meyer Burger), and stripping of the nitride layer in 5% diluted HF.

Minority carrier lifetimes were measured by photoconductance decay (WCT 120, Sinton Instruments). The spatial uniformity of the minority carrier density was assessed by photoluminescence imaging using excitation at 808 nm and a cooled Si detector (PIXIS, Princeton Instruments).

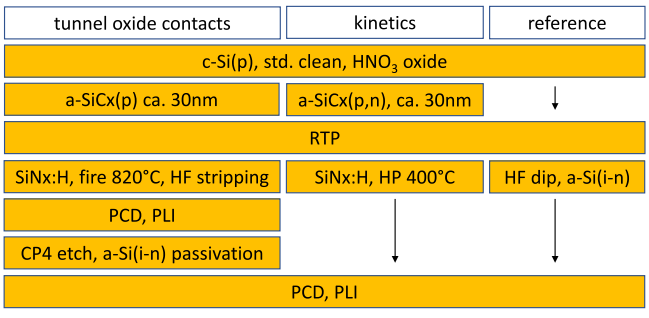

FIGURE 1 | Processing sequence of the different sample structures.

Reference samples for the measurement of the bulk lifetime were subjected to RTP without the growth of the doped SiCx layers, HF dipped to remove oxide and covered with a bilayer of intrinsic and *n*-type amorphous silicon at 200°C (KAI-M, Unaxis). In earlier work, we estimated this to provide near-perfect surface passivation with surface recombination velocity of ~2 cm/s [6]. Alternatively, to assess the impact of hydrogenation on the bulk, the annealed and hydrogenated SiOx/SiCx layer-stack was etched in CP4 solution, and the surfaces were again passivated with bilayers of intrinsic and *n*-type amorphous silicon. On samples exposed to RTP below temperatures of 700°C, we found that this procedure led to blistering during the subsequent firing step of the hydrogenation process, presumably because hydrogen in the SiCx layer was not fully effused during RTP. In the following we show only results for RTP at higher temperatures.

To assess the kinetics of hydrogenation, we replaced the firing step at 820°C by hot-plate annealing up to 30 min at 450°C. This alternative hydrogenation method was also used for solar cell processing.

2.1 | Bulk Lifetime

To assess changes to the bulk lifetime, we use the samples called 'reference'. Figure 2 shows lifetime values extracted at an excess carrier density of 1×10^{15} cm^{-3} to represent the bulk lifetime. In our *p*-type FZ material, this is typically between 2 and 3 ms. The bulk lifetimes are maintained for RTP up to temperatures of about 450°C, followed by a severe decay and eventually a moderate recovery at temperatures above 800°C. The behaviour has been identified with substitutional nitrogen atoms whose defect state is hydrogen passivated; above 450°C, the defect is formed by hydrogen dissociation whereas dissociation of nitrogen from the defect above 800°C gives rise to a partial recovery [5]. Compared to FZ wafers, *p*-type Cz wafers show slightly lower initial bulk lifetimes between 400 and 600 μs, but these values are maintained up to about 600°C. Beyond that temperature, the bulk lifetimes also decay. Whereas the extent of the decay is much less than in the FZ material, there is no recovery at higher temperatures.

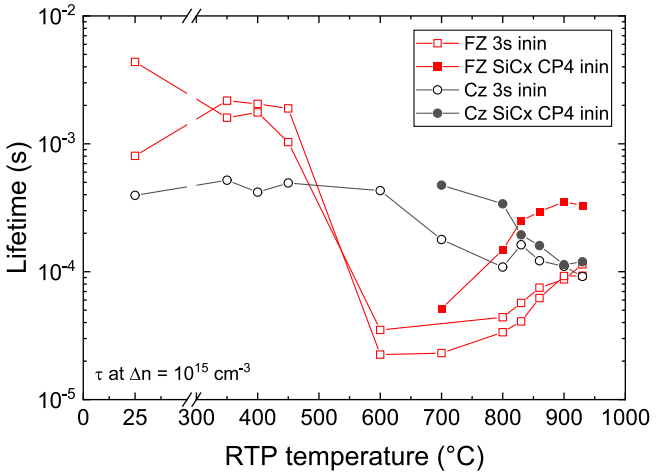

FIGURE 2 | Bulk lifetimes of samples directly after RTP (open symbols) and after additional hydrogenation (above 700°C, full symbols), using FZ wafers (red squares) or Cz wafers (black circles).

Our hydrogenation process can partially passivate the bulk defects in FZ material, but the initial state is not completely recovered. In Cz material, the data in Figure 2 suggest that RTP creates two different types of defects; those created up to 800°C can be effectively passivated by our hydrogen process such that the initial state is recovered, whereas those created at higher temperature cannot be passivated by our hydrogenation process at all.

In an attempt to assess the type of defects, we apply a method proposed by Murphy; for *p*-type material, they showed that SRH recombination at a single defect state yields a linear characteristic in a plot of the lifetime over the ratio $n/p \approx \Delta n/(p_0 + \Delta n)$ [9]. Two independent defects yield two linear branches where rising or falling slopes are indicative of deep and shallow defects, respectively, and the intercept at $n/p \to 1$ yields a positive value for the so-called ambipolar lifetime. We start by removing from our measured minority carrier lifetime data the contributions related to the Auger-effect and radiative recombination [10, 11]. Figure 3 illustrates the resulting characteristics for our FZ and Cz samples. We apply a fitting routine that assumes two independent defects without any constraints. The routine identifies a rising and a falling contribution for all RTP conditions as illustrated by the overlaid curves.

The fitting procedure does not yield a complete characterization of the defects, but only a defect parameter solution surface (DPSS), that is, a relation between the ratio k of the capture cross sections and the energetic position E_t of the defect within the bandgap. The DPSS can be constructed from the slope and the intercept of the linear fitting functions according to equation (2) of ref. [6]. The resulting characteristics for the rising and the falling components are illustrated for the sample that did not receive any thermal treatment (labelled 'none' in Figure 4).

For the Cz wafers, the characteristics for the deep defect corresponding to no treatment and for RTP up to 600°C are close to a capture ratio of 10 for energetic positions in the central region of the gap. This is compatible with the characteristic reported for the boron-oxygen complex [12]. For RTP at higher temperatures, the capture ratio drops to values around 2. Figure 4 includes data for those samples of the structure 'tunnel oxide contacts' that did not blister, that is, those exposed to RTP at 700°C and higher. They were measured after hydrogenation, CP4 etch and re-passivation to represent again bulk lifetimes. Thus, they appear to revert to values closer 10, even though Figure 2 suggested that our hydrogenation process does not fully retrieve the initial lifetimes. This could mean that it can passivate the defect state with capture ratio of 2, but it does not effectively passivate the BO-related defect as it is not assisted by the required amount of carrier injection [13].

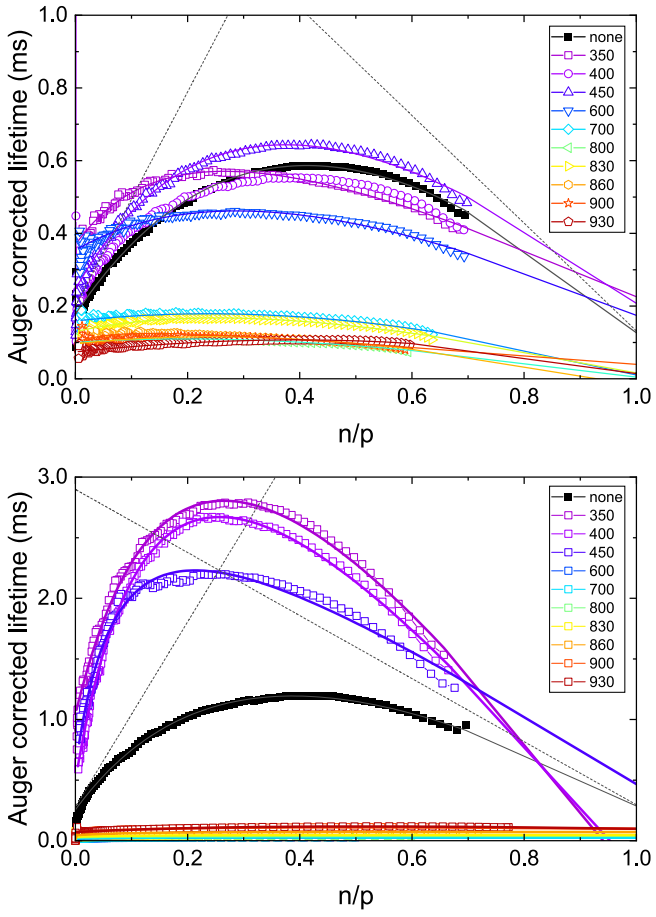

FIGURE 3 | Auger corrected bulk lifetime of the 'reference' samples after RTP, plotted w.r. to the ratio n/p. Upper and lower panels represent Cz and FZ material, respectively. Overlaid are fitting curves for two independent defects, and dashed lines illustrate the components for the samples that were passivated directly w/o RTP.

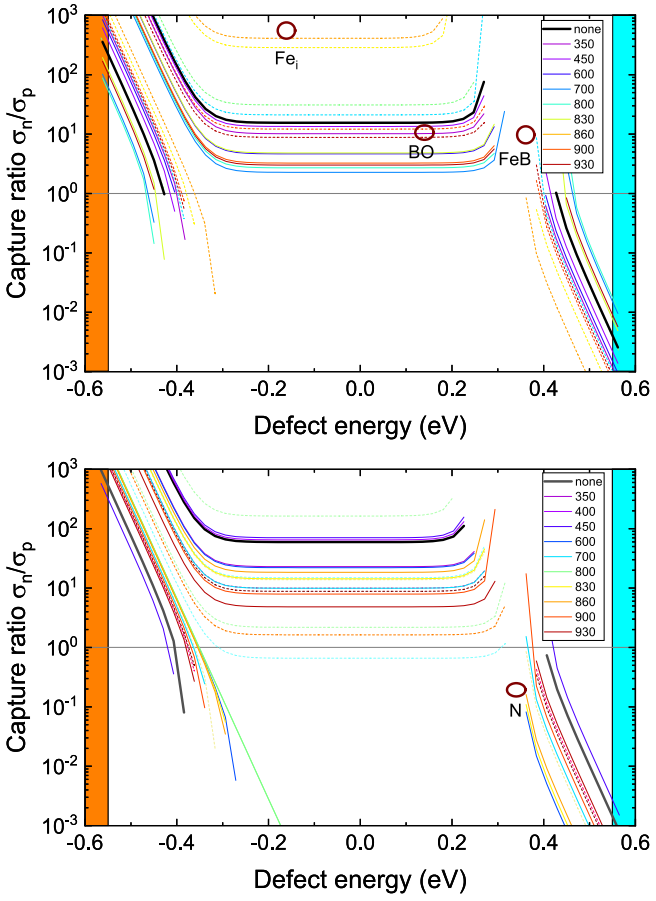

FIGURE 4 | DPSS characteristics for Cz and FZ material (upper and lower panel, respectively). Full lines represent 'reference' samples, and dashed lines denote 'tunnel oxide contacts' after hydrogenation, stripping and re-passivation (due to blistering issues only for RTP above 700°C). Parameters for common defects are illustrated by circles.

For the FZ wafers, no thermal treatment and RTP up to 450°C suggest a capture ratio of around 100. For RTP at higher temperatures, the characteristics scatter rather broadly, but above 900°C, they appear to congregate at a capture of ratio around 10. For the hydrogenated samples exposed to RTP between 700°C and 830°C, the capture ratios scatter and only those subjected to RTP at higher temperatures seem to congregate at a capture ratio around 10. Whereas indictive of the BO-complex, we would not expect oxygen to diffuse into the wafer bulk during the short duration of our RTP, at least not deeper than the region removed by etching in CP4. The characteristics of the shallow defect evaluate to meaningful capture ratios only close to the band edges, but none of them complies well with the nitrogen defect reported for *n*-type FZ material [14].

2.2 | SiOx/SiCx(p) Passivating Contact

For passivating contacts, the wafer surface is covered with a bilayer of SiOx/SiCx(p). As the surface passivation of the bilayer changes with the RTP and also with the subsequent hydrogenation, the effective lifetimes in Figure 5 show the combined effect of defects in the bulk and at the Si/SiOx interface. Different from the bulk lifetimes in Figure 2, the effective lifetimes after RTP start decreasing for temperatures between 830°C and 860°C. Hydrogenation improves the effective lifetimes significantly for RTP at low temperatures, but it becomes less and less effective for RTP above 860°C. In earlier work, we attributed the decay of the effective lifetimes to the formation of pinholes in the interfacial oxide, such that within the pinhole area, the wafer gets into direct contact with defects in the layer of highly doped silicon [6].

Finally, Figure 5 also includes samples where the interfacial oxide was formed in N_2O plasma (stars) [15]. Unfortunately, in this case, the effective lifetimes were measured only after hydrogenation, but the results show clearly that a different oxide formation process can mitigate the adverse effect of pinhole formation, or at least extend its onset towards higher temperatures.

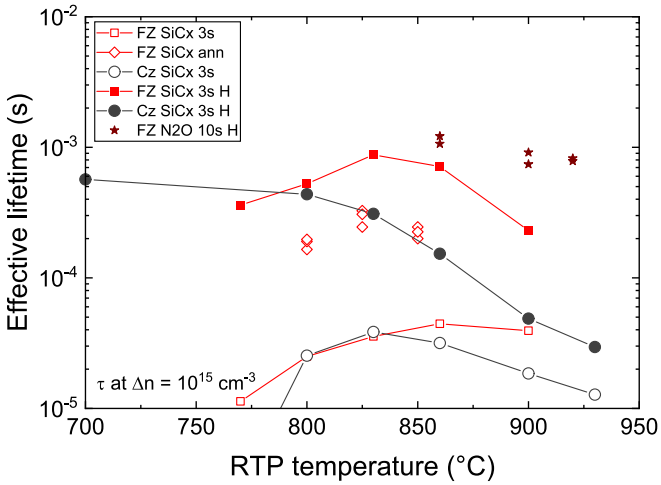

FIGURE 5 | Effective lifetimes of samples corresponding to the RTP series of Figure 2, but covered with a passivating layer stack of SiOx/SiCx(p). Additional data refer to samples with N_2O plasma oxide after RTP (stars).

2.3 | Surface Recombination Velocity

Having access to the effective lifetime and to the bulk lifetime, we can attempt to determine the surface recombination velocity of the Si/SiOx interface. To this end, we use $1/\tau_s = 1/\tau_{eff} - 1/\tau_{bulk}$ to determine τ_s, the contribution of the surface to the effective lifetime. Subsequently, using the wafer thickness w and the bulk diffusivity D, the surface recombination velocity S is obtained as follows [16]:

$$S = \sqrt{\frac{D}{\tau_s}} \cdot \tan\left(\frac{w}{2\sqrt{D\tau_s}}\right) \tag{1}$$

Alternatively, in cases where the effective lifetime is entirely limited by surface recombination at the two surfaces of the wafer, S can be obtained from the saturation current density j_0 as follows [17].

$$S \approx \frac{j_0(p_0 + \Delta n)}{2qn_i^2} \tag{2}$$

Limitation by surface recombination, and thus the applicability of Equation (2), can be identified in the plot of the lifetime over n/p. If limited by surface recombination, Equation (2) also

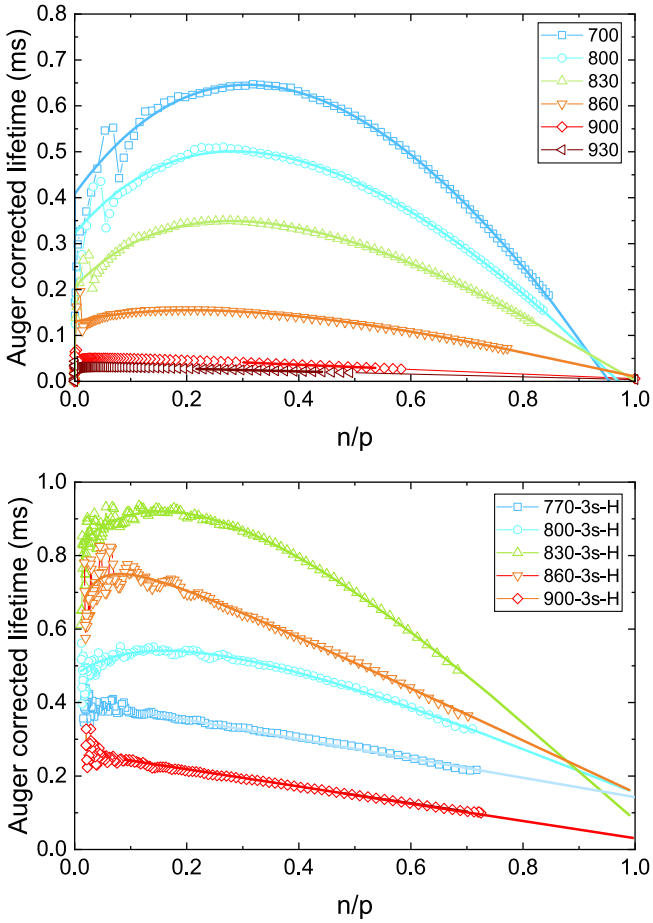

FIGURE 6 | Effective lifetime of 'tunnel oxide contact' samples RTP for 3 s at the indicated temperatures, followed by hydrogenation. Results for Cz wafers and FZ wafers are shown in the upper and lower panel, respectively, and lines denote fitting results.

predicts a linear characteristic with falling slope, but the intercept for $n/p \to 1$ is no longer finite and positive as in the case of shallow defects, but it extrapolates exactly to zero [6]. We find this behaviour for most of the samples before hydrogenation, suggesting that the SiOx/SiCx(p) stack provides poor passivation when the interfacial oxide is not hydrogenated [6]. For the hydrogenated samples in Figure 6, intercepts close to zero are observed for most of the Cz samples, but for the FZ samples appear to show a transition from positive intercepts to values closer to zero as RTP is raised to 900°C, suggesting that in those samples, surface recombination becomes dominant as the interfacial SiOx layer is compromised by pinhole formation.

Figure 7 collects data for S with respect to the RTP temperature. For the samples before hydrogenation, there is a good agreement between Equations (1) and (2), and the variation of S with temperature suggests that increasing temperatures during RTP decrease the defect density at the Si/SiOx interface up to about 830°C. For higher temperatures, S increases due to pinhole formation [18]. The behaviour is very similar for the two wafer types, confirming that S describes properties of the surface without contributions of the bulk.

For the samples after hydrogenation, we could use only Equation (2), and based on the intercept for $n/p \to 1$, we note that it applies best above 860°C where surface recombination through pinholes dominates and hydrogenation is only little effective in this region. Below 830°C, Equation (2) would predict S in the range between 8 and 12 cm/s, but the true values might be even lower.

2.4 | Hydrogenation Kinetics

We investigated the progress of the hydrogenation process with a dedicated set of samples called 'kinetics'. To this end, we used p-type FZ wafer after RTP at 800°C for 3 s. To anticipate the design of a solar cell, we tested SiCx layers of both polarities. Hydrogenation was carried out by hotplate annealing at 450°C instead of firing at 820°C.

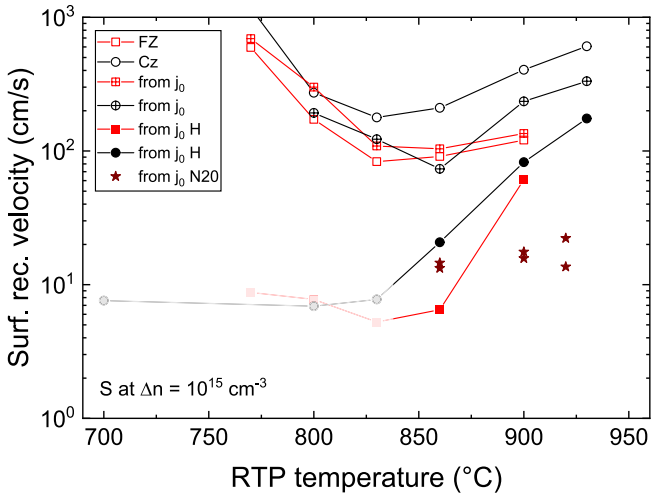

FIGURE 7 | Surface recombination velocities of FZ and Cz wafers (red squares and black circles, respectively) with SiOx/SiCx(p) tunnel contacts after RTP at the shown temperatures (open symbols) and after hydrogenation (full symbols). The greyed region denotes conditions where Equation (2) is no longer applicable. Stars represent interfacial oxides formed by N_2O plasma (measured only after hydrogenation).

From the PL images in Figure 8, we conclude that there are two different reaction kinetics, a fast one for hydrogenation of defects at the Si/SiOx interface and a slow one for hydrogenation of bulk defects. This conclusion is based on work that found the density of thermally generated bulk defects in FZ material to decrease radially from the centre towards the outer regions [19]. Thus, the increased PL signal appearing after 1 min in the ring-shaped region suggests that defects at the Si/SiOx interface are quickly passivated by hydrogenation, making visible the higher bulk lifetime in that region.

If we assume that the improvement of surface passivation proceeds equally fast over the full wafer surface, the low luminescence signal in the centre is then related to the higher density of bulk defects. We find that their response to hydrogenation is much slower, reflecting either the kinetics of hydrogen diffusion in the crystalline bulk, or the reaction kinetics associated to the hydrogenation of the bulk defects.

Figure 9 shows the corresponding effective lifetimes, measured in the centre of the wafers. We find that the SiOx/SiCx(p) bilayer already provides a minor degree of surface passivation after RTP with S in the range of 100 to 200 cm/s according to Figure 7. In contrast, for the bilayer with n-type SiCx, the effective lifetimes after RTP are close to the limit of $\tau = (w/\pi)^2/D_n$, which is obtained for $S = \infty$ [20], suggesting that it does not provide any surface passivation at all.

We can tentatively explain this finding by an upward band-bending induced by the p-type SiCx layer, resulting in an accumulation of holes in the wafer and consequently reducing the availability of electrons for recombination through interfacial defects. The n-type SiCx, in contrast, induces a downward band-bending, thus enhancing recombination.

After hydrogenation for only 1 min, the PL signal in Figure 8 suggests that hydrogen passivation of interfacial defects proceeds faster for the n-layer than for the p-layer. Even though the two layers differ slightly in thickness and crystallinity, the observation of hydrogen diffusion being slower in p-Si is consistent with reported work [21].

2.5 | Demonstrator Solar Cell

To test the suitability of the RTP-treated SiOx/SiCx passivating contacts, we manufactured demonstrator solar cells. To this end, we used p-type FZ wafers with single side texture, formed the interfacial SiOx on both sides, and applied n-type and p-type SiCx layers to the front and the rear, respectively. After RTP at 800°C, the cell precursors were hydrogenated like the samples of the 'kinetics' experiment, but for an extended time of 30 min. Finally, five solar cells of 2 cm × 2 cm were defined per wafer by sputtering through shadow masks. On the rear, we used a bilayer of ITO and Ag to form a full area contact. On the front, only ITO was sputtered, followed by screen-printing of Ag grid lines and curing for 30 min at 130°C. The best cell reached an

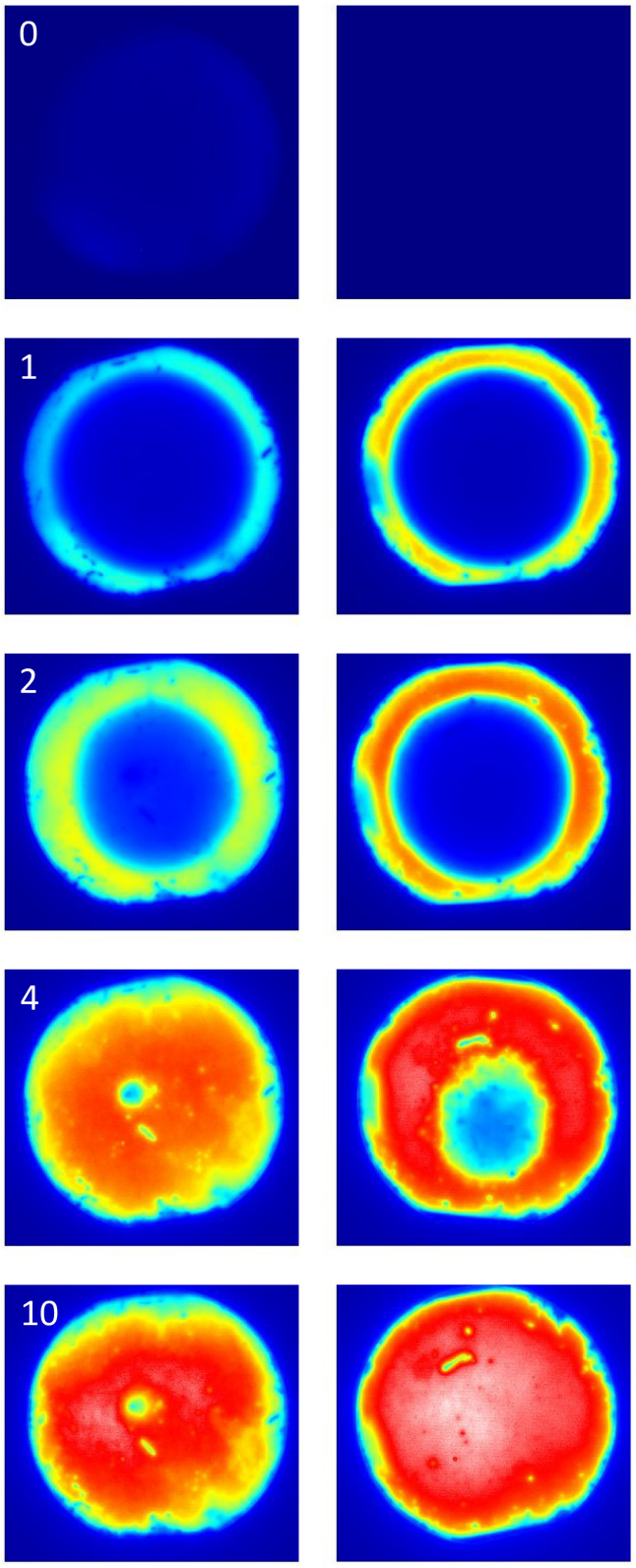

FIGURE 8 | Photoluminescence images of FZ wafers with p-type (left) and n-type (right) passivating contacts after hydrogenation by hotplate annealing for the indicated times between 0 and 10 min.

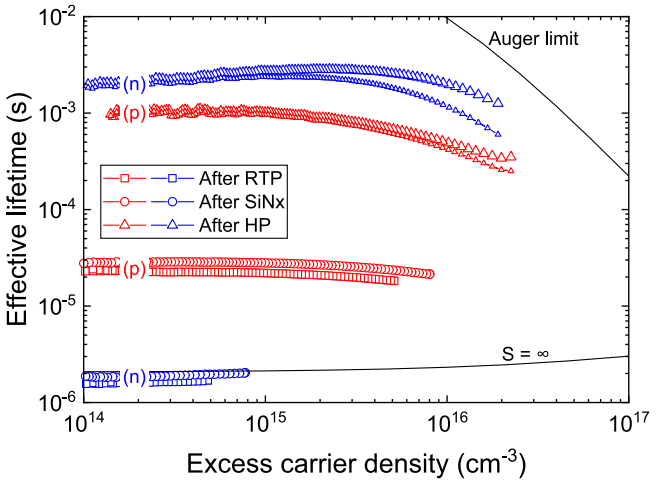

FIGURE 9 | Effective lifetimes of FZ wafers with *p*- and *n*-type passivating contacts shown in Figure 8. Measured after RTP (squares), after SiNx deposition (circles) and after hydrogenation by 30 min of hotplate annealing (small triangles illustrate the measured data before Auger correction).

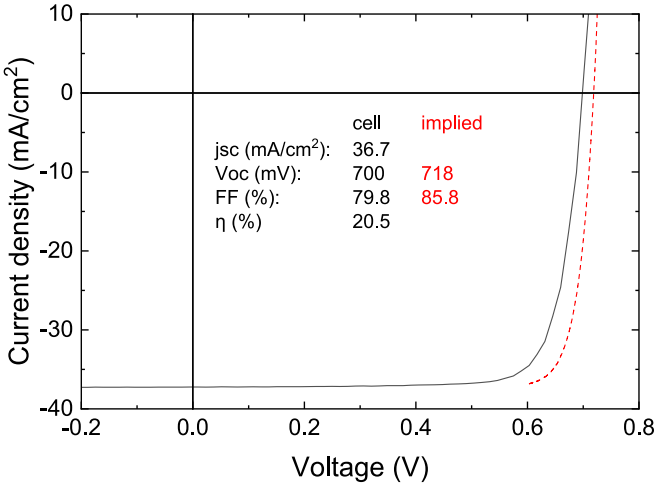

FIGURE 10 | Current voltage characteristics of the best 2 cm × 2 cm demonstrator solar cell, measured after curing at 130°C. The dashed line illustrates the implied $j(V)$ curve before metallization.

efficiency of 20.5%. Figure 10 shows a comparison between the implied $j(V)$ characteristics based on a lifetime measurement just before ITO deposition and the actually measured $j(V)$ characteristics of the best solar cell. The measured efficiency of 20.5% compares favourably to devices with similar design, that is, single-side textured with sputtered ITO contacts on both sides, but using tube furnace annealing instead of RTP [22].

The difference between the implied Voc and the measured Voc of the complete device is likely due to sputtering damage. Regarding the difference between implied FF and measured FF, the contact resistance of the full-area tunnel contact typically varies between 20 and 150 mΩcm^2 for the chosen RTP temperature of 800°C [15, 23] and therefore accounts only for a loss around 0.7% (absolute). The reminder is either due to additional resistive losses by lateral transport in the ITO layer between the finger metallization, or due to the effect of sputter damage on the diode quality factor.

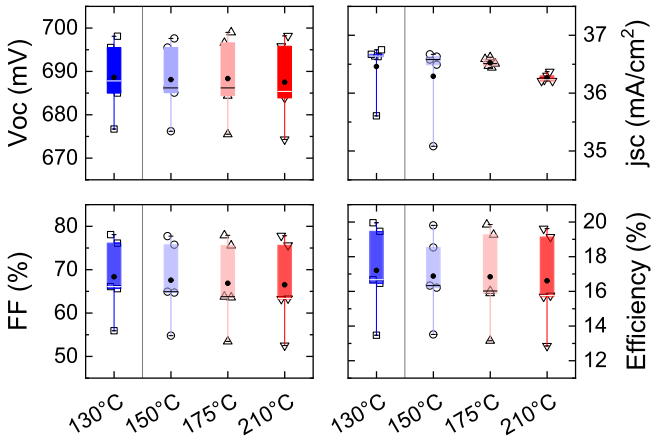

FIGURE 11 | Impact of additional curing steps on the solar cell parameters (statistics of five cells).

Figure 11 shows the impact of additional curing steps up to 210°C. The box plots of the different solar cell parameters represent the average of five cells on a wafer processed identically to the one of Figure 10. We find that sputter damage is not cured in the tested temperature range; however, we do observe a slight decrease of jsc, likely due to increased losses by free carrier absorption in the ITO layer. Similar findings have been reported for TOPCon cells where only the *n*-type rear contact employs a tunnel oxide [24].

3 | Conclusions

We investigated the formation of defects in bulk silicon and at the interface to silicon oxide during rapid thermal processing. We find that Cz and FZ material form different defect types, and they respond differently to hydrogenation by firing of a SiNx:H reservoir layer. The surface passivation provided by tunnel oxide contacts improves with increasing temperature up the onset of pinhole formation. For oxides grown in hot HNO_3, we find the onset between 830°C and 860°C, for interfacial oxide formed in N_2O plasma the onset can be extended towards higher temperatures. Using an interfacial oxide formed in HNO_3 and passivating contacts of both polarities, we used RTP at 800°C, that is, just below the onset of pinhole formation, to manufacture a demonstrator solar cell with device efficiency of 20.5%.

Author Contributions

F.-J. Haug initiated the idea, carried out the defect analysis and wrote the manuscript. M. Lehmann developed the RTP process, studied the hydrogenation kinetics by hot-plate annealing and fabricated the demonstrator device. S. Libraro and A. Morisset contributed the results on N_2O plasma oxidation. E. Genç and J. Hurni provided data related to hydrogenation by firing. C. Ballif is head of the laboratory. All authors were involved in the discussion of the experimental results and contributed to their interpretation.

Acknowledgements

This work has received funding from the Swiss Federal Office for Energy (OFEN) within the project iPrecise (No. SI/502115-01) and the Swiss National Science Foundation (SNF) within the projects NACHOS (No. 200021L_172924/1) and IMPACT (no. 200021_185064). We acknowledge the support from the research and innovation program Horizon 2020 of the European Union within the Marie Skłodowska-Curie grant SLICE (No. 101028491), and we thank the Swiss State Secretariat for Research and Innovation (SERI) for funding the association to the EU-project APOLLO (No. 101122277). Open access publishing facilitated by Ecole polytechnique federale de Lausanne, as part of the Wiley - Ecole polytechnique federale de Lausanne agreement via the Consortium Of Swiss Academic Libraries.

Data Availability Statement

The data and the data treatment underlying this contribution are available on the Zenodo repository under the following DOI: 10.5281/zenodo.12188305.

References

1. H. Lin, M. Yang, X. Ru, et al., "Silicon Heterojunction Solar Cells With up to 26.81% Efficiency Achieved by Electrically Optimized Nanocrystalline-Silicon Hole Contact Layers," *Nature Energy* 8 (2023): 789–799.

2. A. Richter, R. Müller, J. Benick, et al., "Design Rules for High-Efficiency Both-Sides-Contacted Silicon Solar Cells With Balanced Charge Carrier Transport and Recombination Losses," *Nature Energy* 6, no. 4 (2021): 429–438.

3. M. A. Green, E. D. Dunlop, M. Yoshita, et al., "Solar Cell Efficiency Tables (Version 64)," *Progress in Photovoltaics: Research and Applications* 32, no. 7 (2024): 425–441, https://doi.org/10.1002/pip.3831.

4. N. E. Grant, V. P. Markevich, J. Mullins, A. R. Peaker, F. Rougieux, and D. Macdonald, "Thermal Activation and Deactivation of Grown-In Defects Limiting the Lifetime of Float-Zone Silicon," *Physica Status Solidi Rapid Research Letters* 10, no. 6 (2016): 443–447, https://doi.org/10.1002/pssr.201600080.

5. D. Hiller, V. P. Markevich, J. A. T. de Guzman, et al., "Kinetics of Bulk Lifetime Degradation in Float-Zone Silicon: Fast Activation and Annihilation of Grown-In Defects and the Role of Hydrogen Versus Light," *Physica Status Solidi A* 217, no. 17 (2020): 2000436.

6. F.-J. Haug, S. Libraro, M. Lehmann, A. Morisset, A. Ingenito, and C. Ballif, "Impact of Rapid Thermal Processing on Bulk and Surface Recombination Mechanisms in FZ Silicon With Fired Passivating Contacts," *Solar Energy Materials and Solar Cells* 238 (2022): 111647.

7. Y. Huang, M. Liao, Z. Wang, et al., "Ultrathin Silicon Oxide Prepared by In-Line Plasma-Assisted N_2O Oxidation (PANO) and the Application for n-Type Polysilicon Passivated Contact," *Solar Energy Materials and Solar Cells* 208 (2020): 110389.

8. M. Bories, J.-I. Polzin, B. Steinhauser, et al., "Plasma-Assisted N_2O Oxidation (PANO) in an Industrial Direct Plasma Reactor for TOPCon Production," presented at the SiliconPV Conference Proceedings, 2023.

9. J. D. Murphy, K. Bothe, R. Krain, V. Voronkov, and R. Falster, "Parameterisation of Injection-Dependent Lifetime Measurements in Semiconductors in Terms of Shockley-Read-Hall Statistics: An Application to Oxide Precipitates in Silicon," *Journal of Applied Physics* 111, no. 11 (2012): 113709.

10. A. Richter, S. W. Glunz, F. Werner, J. Schmidt, and A. Cuevas, "Improved Quantitative Description of Auger Recombination in Crystalline Silicon," *Physical Review B* 86, no. 16 (2012): 165202–165202.

11. T. Niewelt, B. Steinhauser, A. Richter, et al., "Reassessment of the Intrinsic Bulk Recombination in Crystalline Silicon," *Solar Energy Materials and Solar Cells* 235 (2022): 111467.

12. S. Rein and S. Glunz, "Electronic Properties of the Metastable Defect in Boron-Doped Czochralski Silicon: Unambiguous Determination by Advanced Lifetime Spectroscopy," *Applied Physics Letters* 82, no. 7 (2003): 1054–1056.

13. B. Hallam, P. G. Hamer, N. Nampalli, et al., "Rapid Processing of Boron-Oxygen Defects," *Proceedings of 31st European PVSEC* (2015): 531–535.

14. Y. Zhu, F. Rougieux, N. E. Grant, et al., "Electrical Characterization of Thermally Activated Defects in n-Type Float-Zone Silicon," *IEEE Journal of Photovoltaics* 11, no. 1 (2020): 26–35.

15. S. Libraro, A. Morisset, J. Hurni, et al., "Understanding and Mitigating Resistive Losses in Fired Passivating Contacts: Role of the Interfaces and Optimization of the Thermal Budget," *Solar Energy Materials and Solar Cells* 263 (2023): 112591.

16. T. Otaredian, "Separate Contactless Measurement of the Bulk Lifetime and the Surface Recombination Velocity by the Harmonic Optical Generation of the Excess Carriers," *Solid-State Electronics* 36, no. 2 (1993): 153–162.

17. D. E. Kane and R. M. Swanson, "Measurement of the Emitter Saturation Current by a Contactless Photoconductivity Decay Method," *18th IEEE Photovoltaic Specialists Conference* (1985): 578–583.

18. S. Libraro, L. J. Bannenberg, T. Famprikis, et al., "Development and Characterization of N2O-Plasma Oxide Layers for High-Temperature p-Type Passivating Contacts in Silicon Solar Cells," *ACS Applied Materials & Interfaces* 16 (2024): 47931–47943.

19. F. E. Rougieux, N. E. Grant, C. Barugkin, D. Macdonald, and J. D. Murphy, "Influence of Annealing and Bulk Hydrogenation on Lifetime-Limiting Defects in Nitrogen-Doped Floating Zone Silicon," *IEEE Journal of Photovoltaics* 5, no. 2 (2014): 495–498.

20. A. Sproul, "Dimensionless Solution of the Equation Describing the Effect of Surface Recombination on Carrier Decay in Semiconductors," *Journal of Applied Physics* 76, no. 5 (1994): 2851–2854.

21. A. Herguth and B. Hallam, "A Generalized Model for Boron-Oxygen Related Light-Induced Degradation in Crystalline Silicon," *AIP Conference Proceedings* 1999, no. 1 (2018): 130006-1–130006-4, https://doi.org/10.1063/1.5049325.

22. G. Nogay, C. Ballif, A. Ingenito, et al., "Crystalline Silicon Solar Cells With Coannealed Electron- and Hole-Selective SiCx Passivating Contacts," *IEEE Journal of Photovoltaics* 8, no. 6 (2018): 1478–1485, https://doi.org/10.1109/JPHOTOV.2018.2866189.

23. F.-J. Haug, A. Ingenito, F. Meyer, et al., "Contributions to the Contact Resistivity in Fired Tunnel-Oxide Passivating Contacts for Crystalline Silicon Solar Cells," *IEEE Journal of Photovoltaics* 9, no. 6 (2019): 1548–1553.

24. L. Tutsch, F. Feldmann, M. Bivour, W. Wolke, M. Hermle, and J. Rentsch, "Integrating Transparent Conductive Oxides to Improve the Infrared Response of Silicon Solar Cells With Passivating Rear Contacts," presented at the AIP Conference Proceedings, AIP Publishing, 2018.